

Viscous influences on jetting process from an impacted concave free surface

Xiang-Gang Cheng¹ and Xiao-Peng Chen,^{*}¹ Hang Ding,³ Chun-Yu Zhang,³ Jiao-Jiao Guo,² Lai-Bing Jia.⁴

¹School of Marine Science and Technology, Northwestern Polytechnical University, Xi'an, China 710072

²School of Mechanics, Civil Engineering and Architecture, Northwestern Polytechnical University, Xi'an, China 710129

³Department of Modern Mechanics, University of Science and Technology of China, Hefei, China 230027

⁴Department of Naval Architecture Ocean and Marine Engineering, University of Strathclyde, Glasgow, G4 0LZ United Kingdom

Abstract

A focused jet is generated from a concave free surface through an impact of a tube. Experimental and numerical studies were conducted to explore the viscous influences. The results show that a strong vorticity sheet is generated along the free surface just after impact, and the liquid bulk is initialized ($t \leq 10^{-4}$ s). After the impact, the liquid surface evolves freely and a jet is ejected ($t \gg 10^{-4}$ s). Pronounced tangential flow is found, and the material in the jet mainly originates from the viscous penetrating layer below the free surface. According to the above observations, a vorticity mechanism of the free surface evolution is proposed. Further, by combining the viscous and interfacial tension effects, a scaling relation estimating the jetting velocity is derived, which agrees with the numerical and experimental results well. The work will be valuable for viscous droplets preparation.

1 INTRODUCTION

To generate micro-scale jets or produce droplets on demand is a key issue in industrial applications, such as inkjet printing [1], needle-free injection [2, 3], circuit manufacture [4] and biological tissue printing [5]. Recently, a concave free liquid surface was experimentally found to be able to generate a jet after being impacted by an abrupt impulse [6, 7]. A typical example is to release a tube partially filled with wetting liquid (with a concave free surface) from a certain height. Once the tube impacts onto the rigid substrate, it bounces back, while the liquid surface evolves and a jet is shot. Further, Kiyama et al. [8, 9] found that cavitation bubbles generated in the test tube after strong impact could enhance the jet. The focused-jet phenomenon has also been integrated into laser-induced forward transfer technique, to achieve finer jet/droplet and lower energy consuming [10].

^{*}Corr. Author: xchen76@nwpu.edu.cn

The jetting process can be divided into two stages: an impact stage ($t \leq 10^{-4}$ s) and focused-jetting stage ($t \gg 10^{-4}$ s) [7, 11, 12]. In the impact stage, the liquid undergoes a sudden acceleration. As Antkowiak et al. [6] commented, 'the region of influence of viscosity is concentrated near the free surface and the wall in a thin boundary layer of thickness $\sqrt{\nu\tau}$ (ν is the kinematic viscosity and τ is the impact duration), and there are no viscous effects in the volume'. By applying a pressure gradient due to the inertial force, Antkowiak et al. [6] gave an analytical solution of the (initial) instantaneous velocity in the liquid bulk.

After the impact, the interface evolves freely and a jet is generated, which is named as the focused-jetting stage. In order to interpret the underlying mechanism of the focused-jetting process, several models have been proposed. Based on the experiments and numerical simulations, Tagawa et al. [7, 11] proposed a sink-flow model to estimate the velocity of the jet: an inward velocity is supposed to be imposed on the concave free surface immediately after the impact (neglecting the tangential velocity component along the free surface). The converging flow leads to the increment of the velocity and further causes the occurrence of a jet. According to the above assumptions, a normalized jetting velocity is derived as

$$\beta \equiv V_j/U_0 = 1 + \alpha \cos \theta_s, \quad (1)$$

where V_j and U_0 denote the jetting velocity and the characteristic impact velocity, respectively. θ_s is the contact angle, and α is an adjustable prefactor with the order of unity. Furthermore, Gordillo et al. [13] improved the model by imposing a distributed normal velocity on the free surface, which is obtained from a velocity potential equation subjected to appropriate boundary conditions. Considering the constancy of the flow rate during the jet ejection, a more precise jetting velocity is achieved:

$$\beta = v_{n0}(k^2/(3+k^2))^{-2/3}, \quad (2)$$

where v_{n0} is the normalized initial velocity of the free surface in the central region, and k quantifies the variation of the initial radial velocity along the free surface. Both v_{n0} and k are functions of θ_s . Fitted results show that $v_{n0} \simeq 0.31 \cos \theta_s + 0.90$ and $k^2 \simeq 1.6/\cos \theta_s + 1.33$.

The above theoretical predictions show good agreement with the experimental and numerical results under low viscosity working conditions. While, it should be noted that viscous influence is not concerned. Besides, the viscosity indeed decrease the jet strength [12], and it is expected to play significant roles under certain circumstances [5, 10, 12]. Onuki et al. [12] investigated the viscous effects during the jetting process. According to the numerical results, they verified that there are no viscous effects in the liquid volume in the impact stage firstly. Later, they found that a boundary layer is existed near the side wall during the focused-jetting stage. Therefore, the authors proposed that the boundary layer on the side wall intercepts the focusing flow, which decreases the jet velocity perceivably as $\delta^* \geq 0.1$. δ^* denotes a dimensionless boundary layer thickness.

Onuki et al. [12] explored the viscous influences in the process of jet formation. However, the analysis on the flow details near the free surface (where the jet is generated) was missed in the work, which may be related to the viscous effects. Besides, the jet phenomenon studied by the authors is actually the superposition of the pipe flow and the evolution of the free liquid surface. Therefore, deeper work should be done to explore the free surface evolution and the related viscous influences.

As described by Lundgren and Koumoutsakos [14], a free surface flow is always associated with vorticity evolution. For the focused jet phenomenon, the concave surface will generate a thin but strong vorticity sheet (the thickness, $\delta_0 \sim \sqrt{\nu\tau}$) during impact due to the misalignment of the density and the pressure gradients, which is known as the Richtmyer-Meshkov instability

(RMI) [15, 16]. According to the vortical flow theory, vorticity diffuses into deeper fluid region due to viscosity. As we can see in the present work, the vorticity evolution and tangential flow along the free surface are closely related to viscous damping in the jetting process.

In this paper, we investigated the jetting process through the tube-impact approach by a combination of experiments and numerical simulations. Four liquids with different viscosities were utilized in the experiment. A phase field approach [17, 18, 19, 20] was used in the numerical simulations to gain the flow details. We examine the effects of the liquid viscosity and the characteristic impact velocity on the jet velocity. Our aim is to clarify the mechanism of focused jet generation and the viscous effects, seeking a universal scaling law for the jet velocity at last. The rest of the paper is organized as follows. In Sec. 2, the experimental procedures and numerical setup are introduced. In Sec. 3, the results are analysed accompanied by some additional testing simulations. A physical model is proposed and validated in this section. We summarize our results and draw the conclusions in Sec. 4.

2 METHODOLOGY

2.1 Experimental setup and materials

Our experimental setup followed Ref. [8] as depicted in Fig. 1(a). A test tube was hold by an electromagnet initially and was filled with about $L = 7$ mm depth working liquid. The inner diameter of the tube was $2r_0 = 8$ mm. When the experiment started, the magnet was switched off and the tube falled freely until impacted onto a rigid plate. A jet was then ejected from the free surface. The process was captured by using a high speed camera (Megaspeed-75K) with the recording frequency of 5000 f.p.s. at the resolution of 0.14 mm/pixel. The experiments in each working condition were conducted at least three times for reproducibility. The properties of the liquids utilized in the work (dyed water and silicone oils) are listed in Table 1. The viscosities (ν) were measured by using Vickers viscometers (Shanghai Loikaw Instrument Co. Ltd, China) at about 20°C . The surface tension (γ) was measured by a pendant drop method [21] and the density (ρ) was obtained by weighting certain volume of the liquid.

Table 1: The properties of the working liquids. The dyed water was made by dissolving 0.1 g of red dye (Reactive Red X-3B) in 100 ml distilled water, which was purified with an ultrapure water system (EPED, China). Oils 1-3 are silicone oils.

	$\rho(\text{kg/m}^3)$	$\gamma(\text{mN/m})$	$\nu(\text{mm}^2/\text{s})$
Dyed water	999	63	1
Oil-1	937	20	11
Oil-2	934	19	22
Oil-3	941	20	57

Following Kiyama et al. [8], a characteristic velocity is defined: $\mathbf{U}_0 = \mathbf{V}' - \mathbf{V}_0$ (Fig. 1(a)). $V_0(= \sqrt{2gH})$ is the impact velocity of the tube, where $g(= 9.8\text{m/s}^2)$ and H are gravitational acceleration and the falling height, respectively. V' is the rebounding velocity taken as the average speed of the test tube measured in $\Delta t = 6$ ms after the impact (Fig. 2(a)). In the experiment, U_0 ranges in $0.7 \sim 2.3$ m/s corresponding to the falling height $H = 15 \sim 130$ mm. After the impact, the free surface deforms abruptly and a jet is shot. An averaged jetting velocity, V_j , in Δt was measured for analysis (Fig. 2(a)). It should be noted that V_j is evaluated in the coordinate fixed on the tube, and a normalized jet velocity is defined as $\beta \equiv V_j/U_0$.

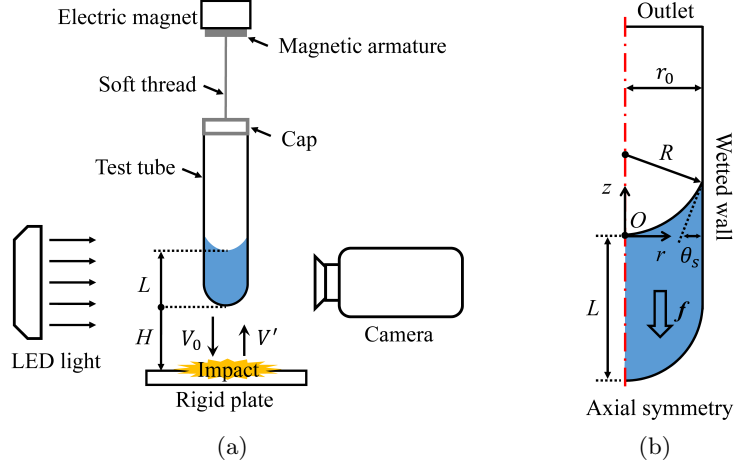


Figure 1: (a) A schematic of the experimental setup. V_0 and V' indicate the impact and rebounding velocity of the tube, respectively, and $\mathbf{U}_0 = \mathbf{V}' - \mathbf{V}_0$. (b) A diagram of the numerical model. The contact angle, $\theta_s = 20^\circ$ for silicone oils and $\theta_s = 13^\circ$ for dyed water. In the simulation, a virtual impulsive force is applied to simulate the impact: $f(t) = a \exp \left[\frac{-(t-\tau/2)^2}{2c^2} \right]$, where $\tau = 1\mu s$, $c = 1/6$, and a is determined by the momentum conservation during the impact.

2.2 Numerical model

The numerical simulations were conducted by using a commercial software, COMSOL. The coordinate system is fixed on the test tube, and a virtual (downward) impulsive inertia force (\mathbf{f}) is imposed on the liquid bulk to simulate the impacting process (Fig. 1(b)). $f(t) = a \exp \left[\frac{-(t-\tau/2)^2}{2c^2} \right]$, where the impact duration $\tau = 1\mu s$ is adopted according to the comparison of the numerical results with the experiments, $c = 1/6$, and a is determined by the momentum conservation during the impact, $\int_0^\tau f(t)dt = \rho U_0$. The wetted wall boundary condition was used on the inner wall of the test tube. The contact angle, $\theta_s = 20^\circ$ for silicone oils and $\theta_s = 13^\circ$ for dyed water, which are determined by measuring the profile of the free surface just before impact.

A phase field approach was used in this study [17, 18, 19, 20]. In this method, a phase index ϕ is defined, and $\phi = 1$ in the liquid phase, $\phi = -1$ in the gas phase, $-1 < \phi < 1$ across the liquid-gas interface. The interface is updated according to the Cahn-Hilliard equation:

$$\frac{\partial \phi}{\partial t} + \mathbf{u} \cdot \nabla \phi = \nabla \cdot (M \nabla G), \quad (3)$$

where \mathbf{u} is velocity, M is the mobility parameter which characterizes the diffusion rate of the phase. G is the chemical potential, which is represented as $G = \lambda [-\nabla^2 \phi + \phi(\phi^2 - 1)/\epsilon^2]$. λ is the mixed free energy density and ϵ characterizes the interface thickness. The local properties of the material, such as the density ρ and dynamic viscosity μ , are interpolated as: $\rho = (1 + \phi)\rho_l/2 + (1 - \phi)\rho_g/2$, $\mu = (1 + \phi)\mu_l/2 + (1 - \phi)\mu_g/2$, where the subscripts l and g represent liquid and gas, respectively.

Furthermore, the surface tension term, $G\nabla\phi$, can be applied in the Navier-Stokes equation:

$$\rho \left(\frac{\partial \mathbf{u}}{\partial t} + \mathbf{u} \cdot \nabla \mathbf{u} \right) = -\nabla p + \nabla \cdot [\mu (\nabla \mathbf{u} + (\nabla \mathbf{u})^T)] + G\nabla\phi + \mathbf{f}. \quad (4)$$

In the simulation, we used a triangular mesh with the minimum size of 0.02mm. The interface thickness ϵ was set as 0.05mm, and the sharp-interface limit [17, 18] was fulfilled.

3 RESULTS AND DISCUSSIONS

3.1 A general description of the jetting process

A typical jetting process is shown in Fig. 2. A tube partially filled with some wetting liquid falls freely at a certain height. Before the impact, the free surface usually seems semi-spherical in gravity-free state. The shape of the meniscus is determined by the triple-phase contact angle θ_s (Fig. 2 (a), $t = 0$). Once the tube impacts onto the rigid plate, it bounces back abruptly (with velocity V'). During the impact, the tube and the liquid undergoes an acceleration $a_I \approx U_0/\tau$. An initial velocity field ($\sim U_0$) is induced by the pressure gradient immediately after the impact. Then, the surface near the wall moves down quickly while the surface in the central region moves upward forming the jet. This implies radial/tangential flow occurs in the focused-jetting stage. From the snapshots, the instantaneous velocity of the jet tip can be obtained as in Fig. 2 (b). It is quantitatively shown that the interface gains an initial velocity immediately after the impact and continues accelerating until $t \approx 2$ ms. After that, the jet becomes longer and thinner, with the velocity decreases slowly ($t > 2$ ms in Fig. 2).

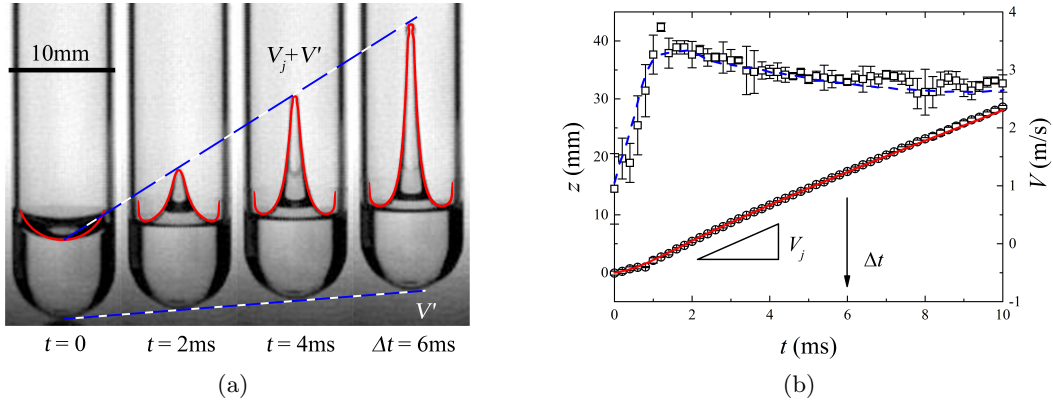


Figure 2: A typical jetting process. The working liquid is Oil-1 and $U_0 = 1.66$ m/s. (a) The evolution of the free surface. The background images show the experiment and the red curves are obtained from the corresponding numerical simulation. The rebounding speed of the tube (V') and jetting speed (V_j) are measured from the snapshots. (b) The jet tip position (\circ) and the instantaneous jetting velocity (\square) in a coordinate system fixed on the tube. The curves represent the corresponding numerical results.

3.2 The viscous influences

By using different liquids and various U_0 , the viscous effects is explored in this section. Fig. 3(a) shows that β decreases with increasing viscosity or decreasing U_0 .

According to Fig. 2(b), one can see that the impact stage is extremely short ($\tau \approx 1 \mu s$) and the variables evolve very fast. Therefore, the balance between the inertial and pressure gradient dominate in this stage, and the viscous effects in the liquid bulk can be neglected:

$$\left(\frac{\partial u}{\partial t}, -\frac{1}{\rho} \nabla p \right) \approx \frac{U_0}{\tau} \gg \nu \frac{U_0}{r_0^2}, \text{ with } \tau \sim 10^{-6}, r_0 \sim 10^{-3}. \quad (5)$$

The viscosity mainly play roles in the focused-jetting stage [12]. As shown in Fig. 2(b), the instantaneous jet velocity V will decrease slowly after it reaches a maximum value, which is related to the viscous and interfacial tension effects. Although Onuki et al. [12] proposed that the boundary layer on the wall may influence the jetting process, there is no perceivable axial flow in our study. On the other hand, we define a Reynolds number, $Re = r_0 U_0 / \nu$, which ranges from 49 to 7667. It implies the viscous dissipation can be roughly neglected compared to the kinetic energy. However, such observation can not be used to explain the β variations: Fig. 3(a) shows that Oil-3 jets gain only about 30% kinetic energy as much as water, while the dissipation rates ($\propto 1/Re$) are about 0.02 and 10^{-4} for Oil-3 and Dyed water, respectively. Therefore, the flow details near the free surface should be considered in analysing the viscous effects.

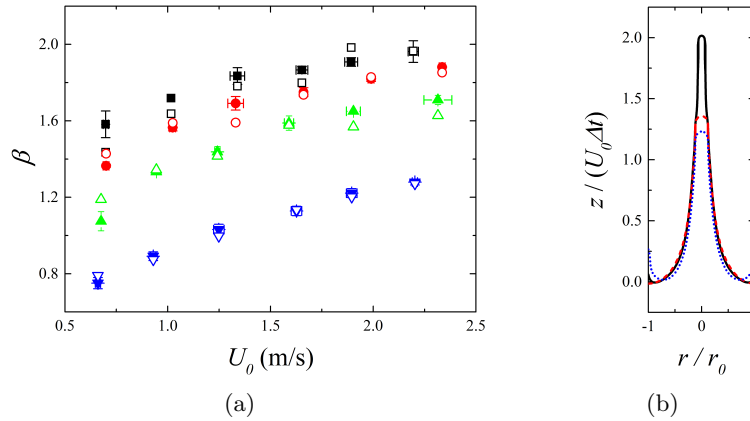


Figure 3: (a) $\beta - U_0$ relations for various liquids (Dyed water (squares), Oil-1 (circles), Oil-2 (triangles), Oil-3 (downward-triangles)). The closed symbols and the open ones represent experimental and numerical results, respectively. (b) Normalized jet profiles for three cases with different viscous conditions. The dotted, dashed and the solid curves correspond to the tested Cases 1-3, respectively.

We first design testing simulations to explore where the viscosity matters:

- Case 1: the real working condition of Oil-3 with $U_0 = 2.3 \text{ m/s}$, corresponding to β_1 .
- Case 2: the working parameters are the same as Case 1 except with slipping walls (shear stress free), corresponding to β_2 .

- Case 3: a liquid with very low viscosity ($\sim 0.5 \text{ mm}^2/\text{s}$) is applied to mimic the inviscid flow ($U_0 = 2.3 \text{ m/s}$), corresponding to β_3 .

The results are compared in Fig. 3(b), where $\beta_3 = 2.01$ is close to the inviscid experiments [7, 8, 11]. Both $\beta_2 (= 0.68\beta_3)$ and $\beta_1 (= 0.61\beta_3)$ are obviously smaller than β_3 . However, β_2 is only 10% larger than β_1 , although the later has additional viscous dissipation on the wall. We also simulate Onuki et al.'s process (Fig.7 in reference [12]) with slip wall condition, the jet velocity is suppressed remarkably by the viscosity as well. These indicate the wall boundary layer plays a trivial influence on the jetting process.

Based on Case 1, we track a group of particles initially locating in a layer with the depth of $\delta (= \sqrt{\nu t_c}, t_c = 2r_0/U_0)$ below the free surface (Fig. 4), where δ denotes the characteristic thickness of the viscous penetrating layer during the jetting process. It is found that there is pronounced tangential flow along the free surface and the jet is mainly formed by the material in the viscous penetrating layer ($t = 3 \text{ ms}$). Then, a new Reynolds number is defined, $Re_p = U_0\delta/\nu = 2(r_0/\delta) = 2/\delta^*$, in order to describe the tangential flow. Re_p ranges from 10 to 124 in the present study, which is reasonable for Fig. 3(a). The viscous influences in the penetrating layer can be further perceived from the vorticity field shown in Fig. 4. An extremely thin vortex sheet appears along the free surface right after the impact ($t = 1\mu\text{s}$). When the free surface evolves, the vorticity diffuses into deeper fluid region ($t = 0.5, 1, 3 \text{ ms}$).

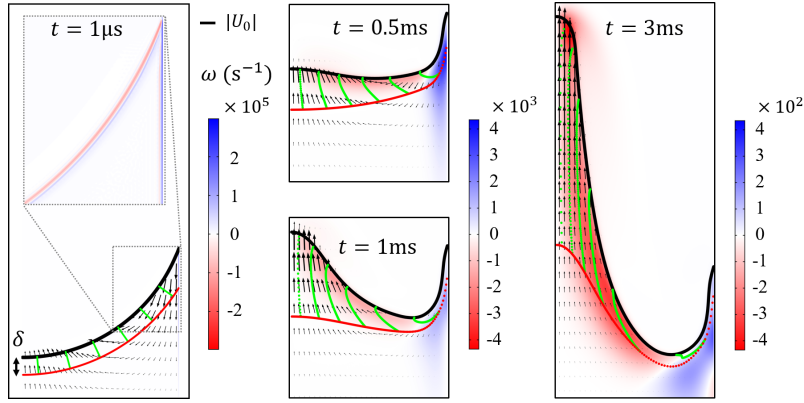


Figure 4: Snapshots of the surface profile (the black thick curves) and vorticity evolutions for Case-1 simulation. The red and green points are tracked particles, which locate in a layer below the free surface initially with a depth of δ (the viscous penetrating depth). The bar shows the velocity scaled as U_0 . A thin vortex sheet is generated just after impact ($t = 1\mu\text{s}$). The panels of $t=0.5\text{ms}$ and $t=1\text{ms}$ share the same color legend of vorticity. Panel-3ms shows that the jet is mainly formed by the liquid particles originated from the viscous penetrating layer.

Accordingly, the viscosity only matters in the focused-jetting stage, and viscous damping occurs in the viscous penetrating layer below the free surface.

3.3 A model for the jetting process

According to the present observations, a simplified model is proposed as illustrated in Fig. 5. Two stages contribute the jetting process sequentially. In the impact stage, the liquid bulk undergoes an acceleration $a_I \approx U_0/\tau$ and a downward pressure gradient ($\nabla p \sim \rho a_I$) is established. Due to the misalignment of the density and the pressure gradients along the free surface (except the

In the focused-jetting stage, the free surface is accelerated due to the vorticity field and strong tangential flow is found (see Fig. 4). Now we turn to the velocity increase of the free surface due to the vorticity (Fig. 5). Assuming the fluid particle on the free surface, M , has a vorticity of $\omega (\approx \omega_0 \cos \theta)$, which contributes a velocity increment $\Delta \mathbf{u}$ to the fluid particle O at the center of the free surface.

where \mathbf{x} is the vector from point O to M , and s is the module of \mathbf{x} , $s=2R\sin\eta$. dV' denotes the volume of M , $dV' = \delta \cdot R d\theta$. Integrating the contribution of the entire vortex sheet to the velocity increment, which is stated as:

where Δu_n is the normal component of $\Delta \mathbf{u}$, $\Delta u_n = \Delta u \cos \eta$. Then Eq. 7 becomes:

where g is a function of θ_s , $g = -\{2\cos(\theta_s/2 + \pi/4) \cdot [\cos^2(\theta_s/2 + \pi/4) - 3]\}/3$. The product of ω_0 and δ is named as the vorticity density, which can be determined by the velocity discontinuity on both sides of the vortex layer. Simply, we estimate the term $\omega_0\delta$ as U_I . The increase in velocity due to vorticity is then

The maximum jet velocity is the sum of the initial velocity just after impact and the velocity increment due to the vorticity field:

8

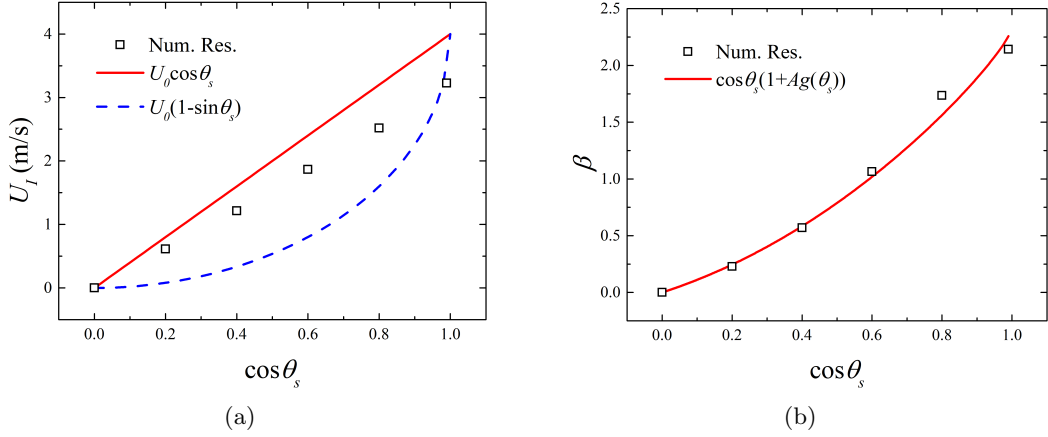


Figure 6: The influence of contact angle. The symbols are the numerical results with $U_0=4.0\text{m/s}$, $Re = 1.6 \times 10^4$, $We = 2 \times 10^4$. (a) The free surface initial velocity, U_I . The curves are the empirical predictions. (b) The curve is the fitting result of Eq.11 with the prefactor of $A = 1.14$.

where A is a prefactor of order unity. One has the normalized jet velocity

$$\beta_0 = \frac{V_j^0}{U_0} = \cos \theta_s(1 + Ag(\theta_s)). \quad (11)$$

Numerical simulations were did with different contact angles. The characteristic velocity U_0 is set as 4.0m/s , and the Reynolds number and the Weber number are large enough to neglect the viscous and interfacial tension effects ($Re = 1.6 \times 10^4$, $We = 2 \times 10^4$). Theoretical fitting result by using Eq.11 shows good agreement with the numerical datas, with a best fitting parameter $A = 1.14$ (Fig. 6(b)).

3.4 Correction for the jet velocity

The above analysis shows the establishing of the velocity field without considering the viscous and interfacial tension effects. However, the viscous and interfacial tension effects indeed decrease the jet velocity (see Figs. 2(b), 3(a)). Firstly, we noticed that both contributions in Eq. (10) will be influenced by the viscosity: the initial velocity will be damped during the evolution and the vorticity will be diffused leading to lower velocity increment. Therefore, a damping factor, $1 - e^{-\frac{t_c}{\Delta t} Re_p}$, is applied to Eq. (11) :

$$\beta' = \frac{V_j'}{U_0} = (1 - e^{-\frac{t_c}{\Delta t} Re_p})\beta_0, \quad (12)$$

where β' and V_j' are intermediate parameters which are only affected by viscosity. Because there is always interfacial tension influence in the experiments, β' can not be measured directly.

To model the interfacial tension, the flow field is first observed carefully as in Fig. 4-3 ms. Two assumptions are adopted: the jet is considered as a cylinder with the radius of r_j and height $V_j \Delta t$, respectively; the upward velocity increases linearly along the jet with a maximum

of V_j (V'_j) at the jet head and zero at its root. The conversion from kinetic energy to interfacial energy is expressed as

$$\frac{\pi}{2} \rho r_j^2 \int_0^{V_j \Delta t} \left[\left(\frac{V'_j}{V_j} \right)^2 - 1 \right] \cdot \left(\frac{z}{\Delta t} \right)^2 \cdot dz \approx 2\pi r_j V_j \Delta t \gamma, \quad (13)$$

deriving Eq.13, a relation is achieved:

$$(\beta')^2 - \beta^2 \approx \frac{12}{We} \frac{r_0}{r_j}, \quad (14)$$

where the Weber number, $We = \rho r_0 U_0^2 / \gamma$, ranges from 31 to 1040 in the present study.

Further using the empirical geometrical condition, $r_j/r_0 = \frac{1}{8} \left(\frac{2}{\beta} \right)^2$ (see Appendix), Eqs. (12) and (14) lead to

$$\beta = \frac{1}{\sqrt{1 + 24We^{-1}}} \beta' = \frac{1 - e^{-\frac{t_c}{\Delta t} Re_p}}{\sqrt{1 + 24We^{-1}}} \beta_0. \quad (15)$$

Accordingly, measured β can be transformed to β' . Fig. 7 (the inset) shows β' obtained from the measured β -data are satisfied by the Eq. (12) with the best fitting parameter $t_c/\Delta t = 0.05$. Furthermore, the $\beta - 1/Re_p$ relations are presented, which implies the necessity of introducing β' : the β -data do not fall on a reduced curve given various interfacial tension. In the figure, we also include Onuki et al. [12]'s data for silicone oils covering a more wider Re_p range. As been shown, Eq. (15) agrees with the measured data, where $\theta_s = 20^\circ$ and $We^{-1} = 0$ are adopted (without knowing the details of Onuki et al. [12]'s data).

Therefore, our study shows the importance of the tangential flow in the focused-jetting process, which makes the dissipation mainly occur in a layer below the free surface. It is also shown that both viscosity and interfacial tension should be concerned in estimating the jetting speed.

4 CONCLUSIONS

We investigate the jetting process in tube-impact approach through experiments and numerical simulations. To clarify the influence of viscosity, two stages, namely the impact and focused-jetting stage, are analysed carefully. In the impact stage, the fluid in the tube undergoes a sudden acceleration, and a thin layer of vortex-sheet is generated on the free surface due to the Richtmyer-Meshkov instability. The flow field is initialized in the stage. In the focused-jetting stage, the free surface evolves following the distributed vorticity and a jet is generated. That results in significant tangential flow and the viscous dissipation near the free surface plays an important role. Based on a relation of $\beta_0 = \cos\theta_s(1 + Ag(\theta_s))$ proposed for an ideal jetting process (with zero surface tension and viscosity), two factors, $(1 - e^{-\frac{t_c}{\Delta t} Re_p})$ and $1/\sqrt{1 + 24We^{-1}}$, are introduced to describe the viscous and interfacial tension effects, respectively, resulting a prediction: $\beta = \frac{1 - e^{-\frac{t_c}{\Delta t} Re_p}}{\sqrt{1 + 24We^{-1}}} \beta_0$, which matches both our and Onuki et al. [12]'s data well.

This work reveals the underlying physics of the generation of focused jet and the viscous effects, which can provide theoretical fundamental for preparing highly viscous or compound droplets etc.

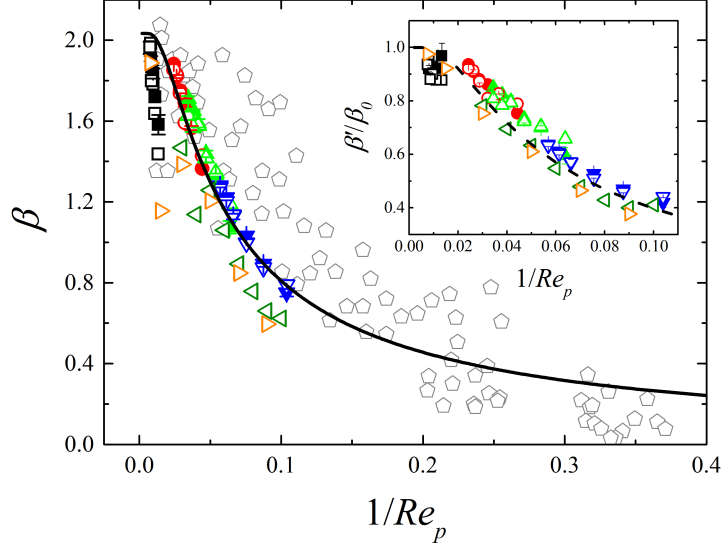


Figure 7: The $\beta - 1/Re_p$ relation. The predicted result (the solid curve) by Eq. (15) with $\theta_s = 20^\circ$ and $We^{-1} = 0$. $t_c/\Delta t = 0.05$ are obtained by fitting predicted β' -data (see the inset). The symbols are presented in the same way as Fig. 3(a). Additional data from Ref. [12] are included (\diamond). The left- and right-triangles show the additional numerical results with $\gamma = 63$ and 80 mN/m, respectively. The inset shows the $\beta'/(\cos\theta_s(1 + Ag(\theta_s)))-1/Re_p$ relation. Our data are fitted by Eq. (12).

ACKNOWLEDGEMENTS

We acknowledge support from the National Natural Science Foundation of China (11872315).

DECLARATION OF INTERESTS

The authors report no conflict of interest.

APPENDIX

Tagawa et al. [7, 11] found the jet radius (r_j) has an order of $O(r_0/10)$. As shown in Eq.14, a more accurate expression for r_j is required for an accurate and compact prediction of jetting speed, and we find an empirical relation: $\frac{r_j}{r_0} \sim b \left(\frac{2}{\beta}\right)^2$, where b is a prefactor with the order of $O(1/10)$. The term of $2/\beta$ implies r_j varies as the jet grows. In Fig.A-1 (a), we measured r_j at $t = \Delta t$, which shows that the relation is generally satisfied. Because the prefactor b also depends on viscosity, we present two values in Fig.A-1 (a) ($1/8$ and $1/13$), which are obtained by fitting the formula to the low viscosity fluids (dyed water and Oil-1) and all the data points, respectively. Further, the final fitting results of β' are in fact insensitive to the b -value (Fig.A-1 (b)), then a relation of $r_j/r_0 = \frac{1}{8} \left(\frac{2}{\beta}\right)^2$ was used.

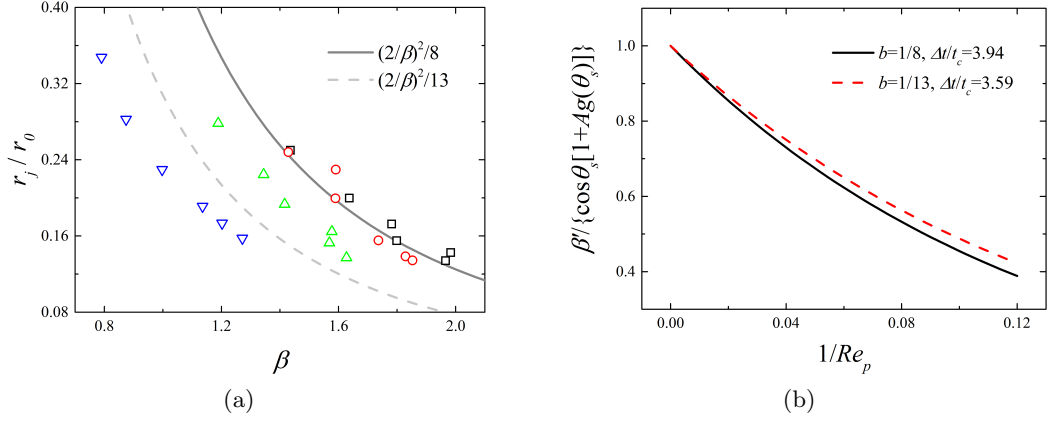


Figure A-1: (a) The measured jet radius. The symbols are presented in the same way as Fig. 3(a). The solid curve and the dashed curve show the fitted results using the data of dyed water and oil-1, and all the numerical datas, respectively. (b) The influence of the geometrical description on the prediction of jetting speed.

References

- [1] M. Singh, HM. Haverinen, P. Dhagat, and GE. Jabbour. Inkjet printing-process and its applications. *Adv. Mater.*, 22(6):673–685, 2010.
- [2] A. Kiyama, N. Endo, S. Kawamoto, C. Katsuta, K. Oida, A. Tanaka, and Y. Tagawa. Visualization of penetration of a high-speed focused microjet into gel and animal skin. *J. Visualization*, 22(3):449–457, 2019.
- [3] N. Kyriazis, P. Koukouvinis, and M. Gavaises. Numerical investigations on bubble-induced jetting and shock wave focusing: application on a needle-free injection. *Proc. R. Soc. A*, 475(2222):20180548, 2019.
- [4] L. Huang, Y. Huang, J. Liang, X. Wan, and Y. Chen. Graphene-based conducting inks for direct inkjet printing of flexible conductive patterns and their applications in electric circuits and chemical sensors. *Nano Res.*, 4(7):675–684, 2011.
- [5] S. V. Murphy and A. Atala. 3D bioprinting of tissues and organs. *Nature Biotech.*, 32(8):773–785, 2014.
- [6] A. Antkowiak, N. Bremond, S. Le Dizes, and E. Villermay. Short-term dynamics of a density interface following an impact. *J. Fluid Mech.*, 577:241–250, 2007.
- [7] Y. Tagawa, N. Oudalov, C. W. Visser, and etc. Highly focused supersonic microjets. *Phys. Rev. X*, 2(3):031002, 2012.
- [8] A. Kiyama, Y. Tagawa, K. Ando, and etc. Effects of a water hammer and cavitation on jet formation in a test tube. *J. Fluid Mech.*, 787:224–236, 2016.
- [9] R. Yukisada, A. Kiyama, X. Zhang, and etc. Enhancement of focused liquid jets by surface bubbles. *Langmuir*, 34(14):4234–4240, 2018.

- [10] E. Turkoz, S. Kang, L. Deike, and C. B. Arnold. Subthreshold laser jetting via flow-focusing in laser-induced forward transfer. *Phys. Rev. Fluids*, 3:082201(R), 2018.
- [11] I. R. Peters, Y. Tagawa, N. Oudalov, C. Sun, A. Prosperetti, D. Lohse, and D. van der Meer. Highly focused supersonic microjets: numerical simulations. *J. Fluid Mech.*, 719: 587–605, 2013.
- [12] H. Onuki, Y. Oi, and Y. Tagawa. Microjet generator for highly viscous fluids. *Phys. Rev. Appl.*, 9:014035, 2018.
- [13] J.M. Gordillo, H. Onuki, and Y. Tagawa. Impulsive generation of jets by flow focusing. *J. Fluid Mech.*, 894:A3, 2020.
- [14] T. Lundgren and P. Koumoutsakos. On the generation of vorticity at a free surface. *J. Fluid Mech.*, 382:351–366, 1999.
- [15] M. Brouillette. The Richtmyer-Meshkov instability. *Annu. Rev. Fluid Mech.*, 34(34):445–468, 2002.
- [16] Y. Zhou. Rayleigh–Taylor and Richtmyer–Meshkov instability induced flow, turbulence, and mixing. i. *Phys. Rep.*, 720–722:1–136, 2017.
- [17] P. Yue, C. Zhou, and J. J. Feng. Sharp-interface limit of the cahn-hilliard model for moving contact lines. *J. Fluid Mech.*, 645:279–294, 2010.
- [18] F.-C. Yang, X.-P. Chen, and P. Yue. Surface roughness effects on contact line motion with small capillary number. *Phys. Fluids*, 30:012106, 2018.
- [19] F.-C. Yang, X.-P. Chen, and P. Yue. The influences of "gas" viscosity on water entry of hydrophobic spheres. *Eur. Phys. J. E*, 42:34, 2019.
- [20] J.-J. Guo, X.-P. Chen, and L. Shui. Surface wave mechanism for directional motion of droplet on an obliquely vibrated substrate. *Phys. Fluids*, 32(3), 2020.
- [21] H. Zhao, D. S. Liu, and X.-P. Chen. Pendant drop method for interfacial tension measurement (in chinese). *J. Exp. Mech.*, 25(1):100–105, 2010.